

The High-Temperature Electrolysis Program at the Idaho National Laboratory: Observations on Performance Degradation

International Workshop on High Temperature Water Electrolysis Limiting Factors

J. E. O'Brien
C. M. Stoots
J. S. Herring
K. G. Condie
G. K. Housley

June 2009

The INL is a
U.S. Department of Energy
National Laboratory
operated by
Battelle Energy Alliance



This is a preprint of a paper intended for publication in a journal or proceedings. Since changes may be made before publication, this preprint should not be cited or reproduced without permission of the author. This document was prepared as an account of work sponsored by an agency of the United States Government. Neither the United States Government nor any agency thereof, or any of their employees, makes any warranty, expressed or implied, or assumes any legal liability or responsibility for any third party's use, or the results of such use, of any information, apparatus, product or process disclosed in this report, or represents that its use by such third party would not infringe privately owned rights. The views expressed in this paper are not necessarily those of the United States Government or the sponsoring agency.

THE HIGH-TEMPERATURE ELECTROLYSIS PROGRAM AT THE IDAHO NATIONAL LABORATORY: OBSERVATIONS ON PERFORMANCE DEGRADATION

J. E. O'Brien, C. M. Stoots, J. S. Herring, K. G. Condie, G. K. Housley
Idaho National Laboratory
Idaho Falls, ID 83415
Tel: (208) 526-1346 , Email: james.obrien@inl.gov

Abstract – *This paper presents an overview of the high-temperature electrolysis research and development program at the Idaho National Laboratory, with selected observations of electrolysis cell degradation at the single-cell, small stack and large facility scales. The objective of the INL program is to address the technical and scale-up issues associated with the implementation of solid-oxide electrolysis cell technology for hydrogen production from steam. In the envisioned application, high-temperature electrolysis would be coupled to an advanced nuclear reactor for efficient large-scale non-fossil non-greenhouse-gas hydrogen production. The program supports a broad range of activities including small bench-scale experiments, larger scale technology demonstrations, detailed computational fluid dynamic modeling, and system modeling. A summary of the current status of these activities and future plans will be provided, with a focus on the problem of cell and stack degradation.*

Introduction

Currently there is increasing interest in the development of large-scale non-fossil hydrogen production technologies. This interest is driven by the immediate demand for hydrogen for refining of increasingly low-quality petroleum resources, the expected intermediate-term demand for carbon-neutral synthetic fuels, and the potential long-term demand for hydrogen as an environmentally benign direct transportation fuel [1]. At present, worldwide hydrogen production is based primarily on steam reforming of methane. From a long-term perspective, methane reforming is not a viable process for large-scale production of hydrogen since natural gas is a non-renewable resource that exhibits large volatility in price and since methane reforming and other fossil-fuel conversion processes emit large quantities of greenhouse gases to the environment. Non-fossil carbon-free options for hydrogen production include conventional water electrolysis coupled to either renewable (e.g., wind) energy sources or nuclear energy. The renewable-hydrogen option may be viable as a supplementary source, but would be very expensive as a large-scale stand-alone option [2]. Conventional electrolysis coupled to nuclear base-load power can approach economical viability when combined with off-peak power, but the capital cost is high [3]. To achieve higher overall hydrogen production efficiencies, high-temperature thermochemical [4] or electrolytic [5] processes can be used. The required high temperature process heat can be based on concentrated solar energy [6] or nuclear energy from advanced high-temperature reactors [7]. Development and demonstration of advanced

nuclear hydrogen technologies are the objectives of the DOE Nuclear Hydrogen Initiative [8].

High-temperature nuclear reactors have the potential for substantially increasing the efficiency of hydrogen production from water, with no consumption of fossil fuels, no production of greenhouse gases, and no other forms of air pollution. Water-splitting for hydrogen production can be accomplished via high-temperature electrolysis (HTE) or thermochemical processes, using high-temperature nuclear process heat. In order to achieve competitive efficiencies, both processes require high-temperature operation ($\sim 850^{\circ}\text{C}$). Thus these hydrogen-production technologies are tied to the development of advanced high-temperature nuclear reactors. High-temperature electrolytic water-splitting supported by nuclear process heat and electricity has the potential to produce hydrogen with overall thermal-to-hydrogen efficiencies of 50% or higher, based on high heating value. This efficiency is near that of the thermochemical processes [9, 10], but without the severe corrosive conditions of the thermochemical processes and without the fossil fuel consumption and greenhouse gas emissions associated with hydrocarbon processes.

A schematic depiction of a high-temperature gas-cooled reactor coupled to a high-temperature electrolysis system is shown in Fig. 1. In this scheme, the primary helium coolant serves as the working fluid to drive a gas-turbine power cycle, which provides the electrical energy required for the high-temperature electrolysis process. In addition, some of the hot helium is used to deliver high-temperature nuclear process heat directly to the endothermic HTE process. The

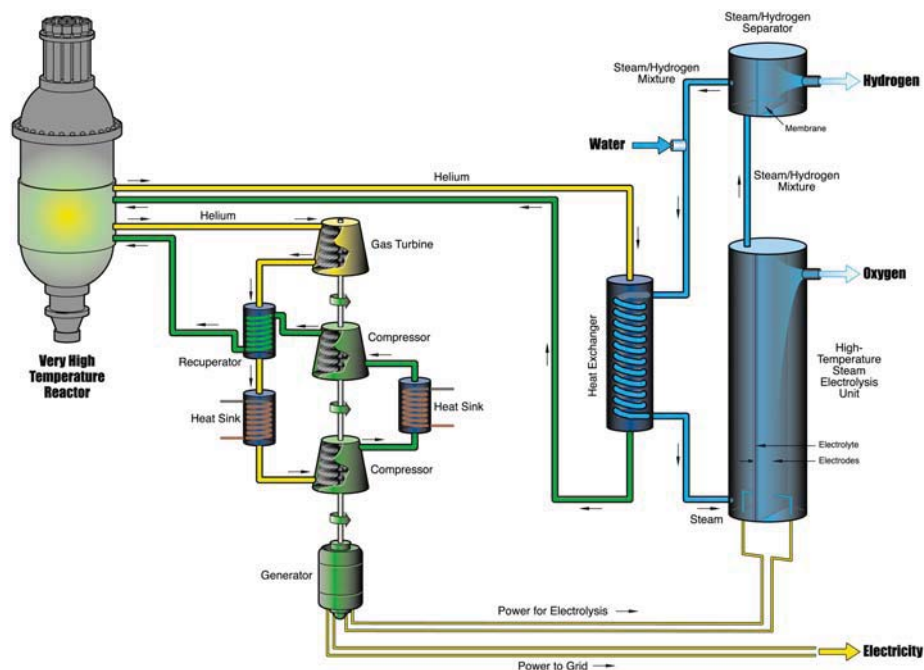


Figure 1. Schematic of high-temperature electrolysis system coupled to an advanced nuclear reactor.

combination of a high-efficiency power cycle and the direct utilization of nuclear process heat yields a high overall thermal-to-hydrogen conversion efficiency of 50% or higher.

A research program is under way at the Idaho National Laboratory (INL) to simultaneously address the technical and scale-up issues associated with the implementation of solid-oxide electrolysis cell technology for efficient hydrogen production from steam. We are coordinating a progression of electrolysis cell and stack testing activities, at increasing scales, along with a continuation of supporting research activities in the areas of materials development, single-cell testing, detailed computational fluid dynamics (CFD) analysis and system modeling.

The INL HTE program also includes an investigation of the feasibility of producing syngas by simultaneous electrolytic reduction of steam and carbon dioxide (coelectrolysis) at high temperature using solid-oxide cells. Syngas, a mixture of hydrogen and carbon monoxide, can be used for the production of synthetic liquid fuels via Fischer-Tropsch processes. This concept, coupled with nuclear energy, provides a possible path to reduced greenhouse gas emissions and increased energy independence, without the major infrastructure shift that would be required for a purely hydrogen-based transportation system [11 - 14]. Furthermore, if the carbon dioxide feedstock is obtained from biomass, the entire concept would be climate-neutral.

HTE System Potential

Detailed process analyses have been performed at INL [10] to analyze HTE-based hydrogen-production systems coupled to advanced nuclear reactors. Overall results from

this study are presented in Fig. 2. This figure shows overall hydrogen production efficiencies, based on high heating value, plotted as a function of reactor outlet temperature. The figure includes a curve that represents 65% of the thermodynamic maximum efficiency, again assuming $T_L = 20^\circ\text{C}$ [15]. Three different advanced-reactor/power-conversion combinations were considered: a helium-cooled reactor coupled to a direct recuperative Brayton cycle, a supercritical CO_2 -cooled reactor coupled to a direct recompression cycle, and a sodium-cooled fast reactor coupled to a Rankine cycle. The system analyses were performed using UniSim [16] software. Each

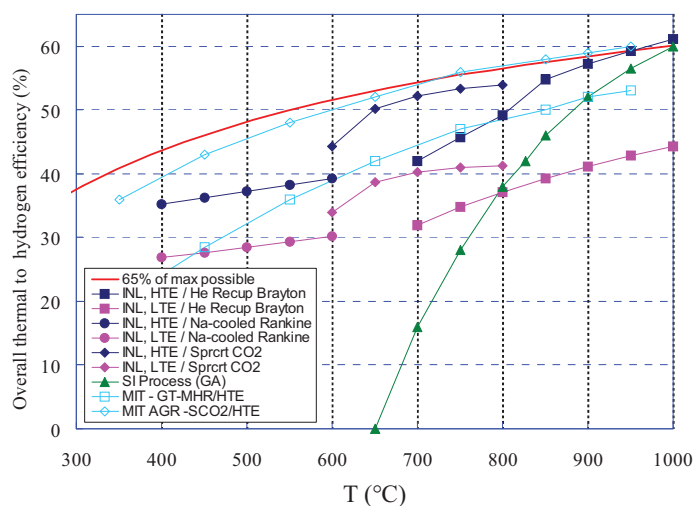


Figure 2. Overall thermal-to-hydrogen efficiencies for HTE coupled to three different reactor types, as a function of reactor outlet temperature.

reactor/power-conversion combination was analyzed over an appropriate reactor outlet temperature range. The figure shows results for both HTE and low-temperature electrolysis (LTE). Results of system analyses performed at MIT [17] are also shown. The lower MIT curve, labeled MIT-GT-MHR/HTE represents overall efficiency predictions for a helium-cooled reactor with a direct Brayton cycle power conversion unit. The upper MIT curve, labeled MIT-AGR-SCO₂/HTE represents overall efficiency predictions for a CO₂-cooled advanced gas reactor with a supercritical CO₂ power conversion unit. Finally, an efficiency curve for the SI thermochemical process [18] is also shown in Fig. 2. The results presented in Fig. 2 indicate that, even when detailed process models are considered, with realistic component efficiencies, heat exchanger performance, and operating conditions, overall hydrogen production efficiencies in excess of 50% can be achieved for HTE with reactor outlet temperatures above 850°C. For reactor outlet temperatures of 600 - 800°C, the supercritical CO₂/recompression power cycle is superior to the He-cooled/Brayton cycle concept. This conclusion is consistent with results presented in [9]. The efficiency curve for the SI process also includes values above 50% for reactor outlet temperatures above 900°C, but it drops off quickly with decreasing temperature, and falls below values for LTE coupled to high-temperature reactors for outlet temperatures below 800°C. Note that even LTE benefits from higher reactor outlet temperatures because of the improved power conversion thermal efficiencies. Current planning for NGNP [7] indicates that reactor outlet temperatures will be at or below 850°C, which favors HTE.



Figure 3. High-temperature electrolysis laboratory at INL – small-scale experiments.

Experimental Program

A photograph of the INL high-temperature electrolysis laboratory is shown in Fig. 3. This part of the laboratory is dedicated to small-scale experiments with single cells and small stacks. The laboratory is currently being upgraded and will soon include three furnaces for single and button cell tests, plus two larger furnaces for stack testing.

A schematic of the experimental apparatus used for single-cell testing is presented in Fig. 4. Primary components include gas supply cylinders, mass-flow controllers, a humidifier, on-line dewpoint and CO₂ measurement stations, temperature and pressure measurement, high temperature furnace, a solid oxide electrolysis cell, and a gas chromatograph. Nitrogen is used as an inert carrier gas.

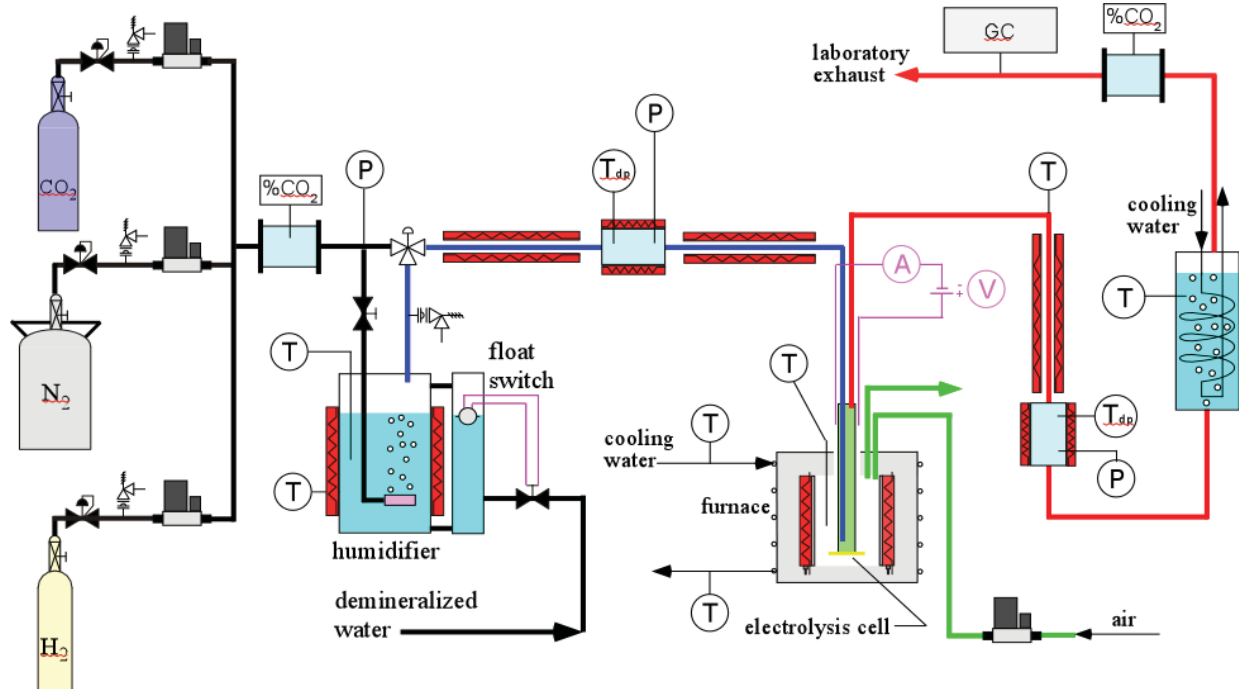


Figure 4. Schematic of single-cell co-electrolysis test apparatus.

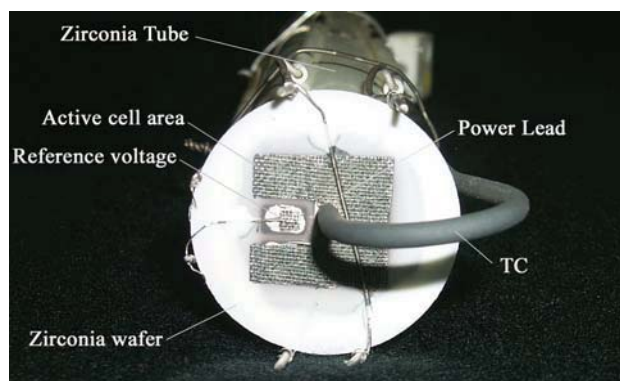


Figure 5. Detail of button cell.

Carbon dioxide and related instrumentation is included for co-electrolysis experiments. Inlet flow rates of nitrogen, hydrogen, carbon dioxide and air are established by means of precision mass-flow controllers. Hydrogen is included in the inlet flow as a reducing gas in order to prevent oxidation of the Nickel cermet electrode material. Air flow to the stack is supplied by the shop air system, after passing through a two-stage extractor / dryer unit. The cathode-side inlet gas mixture, consisting of hydrogen, nitrogen, and possibly carbon dioxide (for coelectrolysis tests) is mixed with steam by means of a heated humidifier. The dewpoint temperature of the nitrogen / hydrogen / CO₂ / steam gas mixture exiting the humidifier is monitored continuously using a precision dewpoint sensor. All gas lines located downstream of the humidifier are heat-traced in order to prevent steam condensation. Inlet and outlet CO₂ concentrations are also monitored continuously using on-line infra-red CO₂ sensors, when applicable.

For single-cell testing, an electrolysis button cell is bonded to the bottom of a zirconia tube, as shown in Fig. 5, using a glass seal. During testing, the tube is suspended in the furnace. The cell shown is an electrolyte-supported single button cell with a scandia-stabilized zirconia electrolyte, about 150 μm thick. The outside electrode, which is exposed to air, acts as the cathode in fuel cell mode and the anode in electrolysis mode. This electrode is a doped manganite. The inside steam-hydrogen electrode (electrolysis cathode) material is a nickel cermet. Both button-cell electrodes incorporate a platinum wire mesh for current distribution and collection. The button cell includes both an active cell area (2.5 cm² for the cell shown) and a reference cell area. The active cell area is wired with both power lead wires and voltage taps. The reference cell area is wired only with voltage taps, allowing for continuous monitoring of open-cell potential. The power lead and voltage wires are routed to the far end of the zirconia tube via several small-diameter alumina tubes fixed to the outside of the zirconia manifold tube. A type-K stainless-steel sheathed thermocouple, is mounted on the manifold tube and bent around in front of the button cell in order to allow for continuous monitoring of the button-cell temperature.

The inlet gas mixture enters this tube, directing the gas to the steam/hydrogen/CO₂ side (inside) of the cell. The cell is maintained at an appropriate operating temperature (800 to 850°C) via computer-based feedback control. The furnace also preheats the inlet gas mixture and the air sweep gas. Oxygen produced by electrolysis is captured by the sweep gas stream and expelled into the laboratory. The product stream exits the zirconia tube and is directed towards the downstream dewpoint and CO₂ sensors and then to a condenser through a heat-traced line. The condenser removes most of the residual steam from the exhaust. The final exhaust stream is vented outside the laboratory through the roof. Rates of steam and CO₂ electrolysis are monitored by the measured change in inlet and outlet steam and CO₂ concentration as measured by the on-line sensors. In addition, a Gas Chromatograph (GC) has been incorporated into the facility downstream of the condenser to precisely quantify the composition of the dry constituents in the electrolysis product stream (including any CH₄ that may be produced).

Results of initial single (button) cell HTE tests completed at the INL were documented in reference [19]. Button cell tests are useful for basic performance characterization of electrode and electrolyte materials and of different cell designs (e.g., electrode-supported, integrated planar, tubular). Polarization curves from reference [19] for several representative DC potential sweeps are presented in Fig. 6. Both the applied cell potentials and the corresponding power densities are plotted in the figure as a function of cell current density. Positive current densities indicate fuel cell mode of operation and negative current densities indicate electrolysis mode. Cell potential values at zero current density correspond to open-circuit potentials, which depend on the furnace temperature and the gas composition. The three sweeps acquired at 800°C (sweeps 1, 3, and 5) have a steeper E-i slope, due to the lower zirconia ionic conductivity at the lower

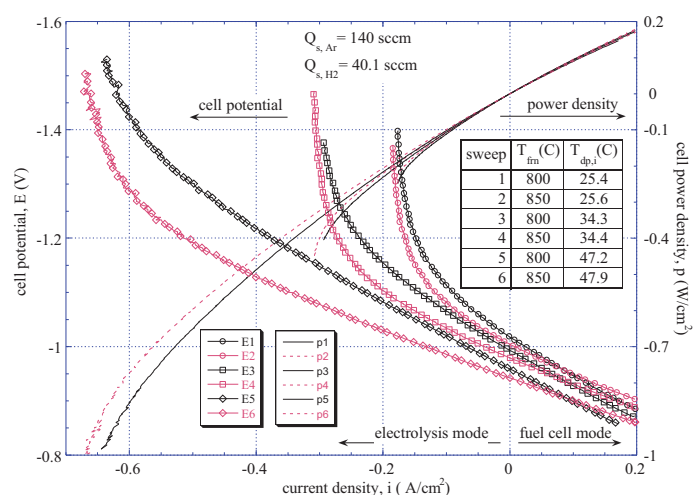


Figure 6. Cell potential and power density as a function of current density.

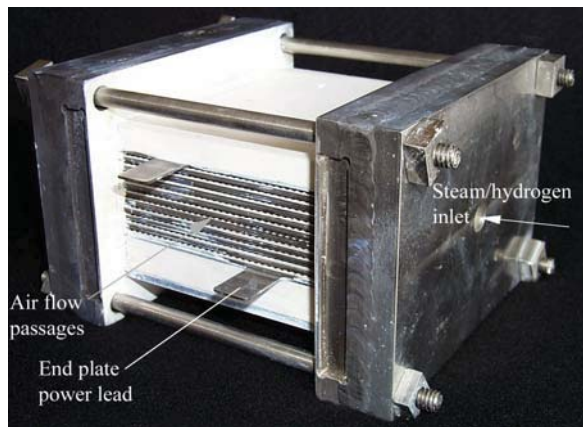


Figure 7. Detail of 10-cell stack.

temperature. The continuous nature of the E-i curves across the zero-current-density (open-circuit) point provides no indication of significant activation overpotential for these electrolyte-supported cells. In the electrolysis mode, the voltage data vary linearly with current density up to a value that depends on the inlet steam flow rate, which for a fixed dry-gas flow rate depends on the inlet dewpoint temperature. For low inlet dewpoint values (sweeps 1 and 2), the voltage begins to increase rapidly at relatively low values of current density ($\sim -0.15 \text{ A/cm}^2$), due to steam starvation. For higher inlet dewpoints, the steam starvation effect is forestalled to higher current densities. The single-cell results demonstrated the feasibility of HTE for hydrogen production linear operation from the fuel-cell to the electrolysis mode.

The majority of the stack testing that has been performed at INL to date has been with planar stacks fabricated by Ceramtec, Inc. of Salt Lake City, UT. A photograph of one of these stacks is provided in Fig. 7 and an exploded view of the internal components is shown in Fig. 8. The cells have an active area of 64 cm^2 . The stacks are designed to operate in cross flow, with the steam / hydrogen gas mixture entering the inlet manifold on the right in the photograph, and exiting through the outlet manifold, visible on the left in the photograph. Air flow enters at the rear though an air inlet manifold (not visible in Fig. 7) and exits at the front directly into the furnace. The power lead attachment tabs, integral with the upper and lower interconnect plates are also visible in the photograph. Stack operating voltages were measured using wires that were directly spot-welded onto these tabs.

Since the stack air outlet plane is not enclosed, the small air flow channels are accessible for instrumentation. Four intermediate cell voltages were monitored using small-diameter wires inserted into these air flow channels. In addition, four miniature thermocouples were inserted into the air flow channels to monitor internal stack temperatures. These were inconel-sheathed, 0.020-inch (508 μm) OD, mineral-insulated, ungrounded, type-K thermocouples.

The internal components of the stack are shown in Fig. 8. The interconnect plates are fabricated from ferritic stainless

steel. Each interconnect includes an impermeable separator plate ($\sim 0.46 \text{ mm}$ thick) with edge rails and two corrugated “flow fields,” one on the air side and one on the steam/hydrogen side. The height of the flow channel formed by the edge rails and flow fields is 1.0 mm . Each flow field includes 32 perforated flow channels across its width to provide uniform gas-flow distribution. The steam/ hydrogen flow fields are fabricated from nickel foil. The air-side flow fields are ferritic stainless steel. The interconnect plates and flow fields also serve as electrical conductors and current distributors. To improve performance, the air-side separator plates and flow fields are pre-surface-treated to form a rare-earth stable conductive oxide scale. A perovskite rare-earth oxide scale is also applied as a bond layer to the separator-plate oxide scale by either screen printing or plasma spraying. On the steam/hydrogen side of the separator plate, a thin ($\sim 10 \mu\text{m}$) nickel metal coating is applied as a bond layer.

The stack electrolytes are scandia-stabilized zirconia, about $140 \mu\text{m}$ thick. The air-side electrodes (anode in the electrolysis mode), are a strontium-doped manganite. The electrodes are graded, with an inner layer of manganite/zirconia ($\sim 13 \mu\text{m}$) immediately adjacent to the electrolyte, a middle layer of pure manganite ($\sim 18 \mu\text{m}$), and an outer bond layer of cobaltite. The steam/ hydrogen electrodes (cathode in the electrolysis mode) are also graded, with a nickel-zirconia cermet layer ($\sim 13 \mu\text{m}$) immediately adjacent to the electrolyte and a pure nickel outer layer ($\sim 10 \mu\text{m}$).

Results of initial short-stack HTE tests performed at INL are provided in references [5, 20]. A good summary of our experience is provided by the results plotted in Fig. 9, from reference [5]. Results of several representative sweeps are shown in Fig. 9 in the form of polarization curves, representing per-cell operating voltage versus current density. Test conditions for each of the seven sweeps are tabulated in the figure. Five of the sweeps were obtained from a 10-cell stack (sweeps 10-1 through 10-5) and two were obtained from

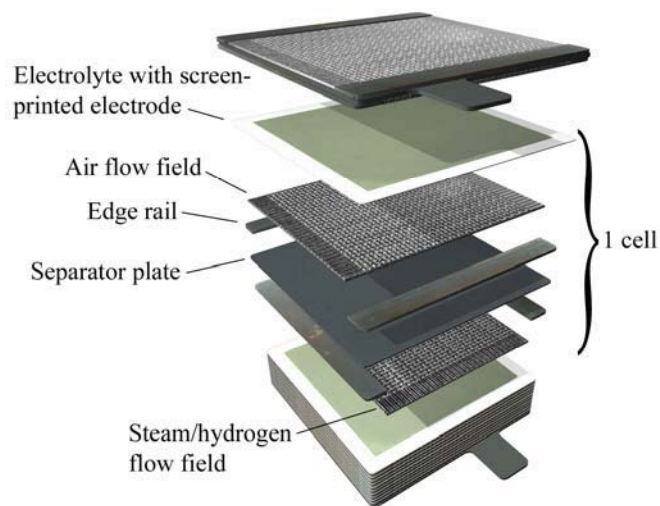


Figure 8. Exploded view of electrolysis stack components.

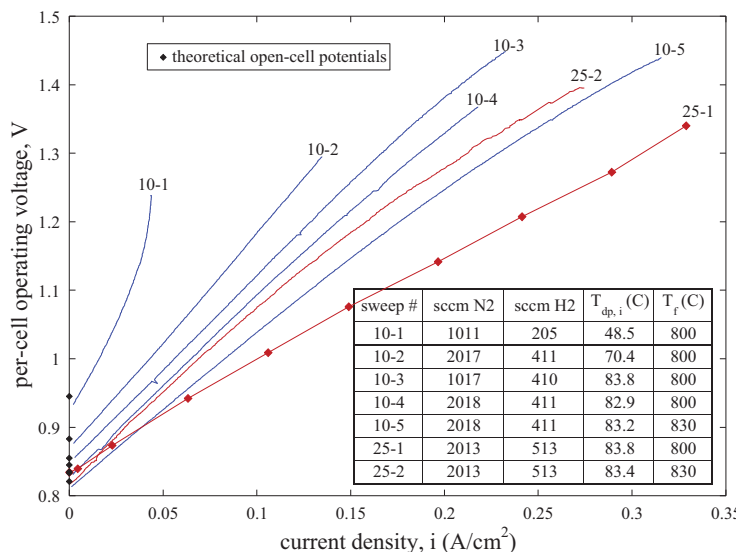


Figure 9. Stack operating potentials as a function of current density, 10-cell stack and 25-cell stack.

a 25-cell stack (25-1 and 25-2). Theoretical open-cell potential values are shown in the figure for each sweep using a single data point at zero current density. Note that the measured open-cell potentials are in excellent agreement with the theoretical values for each sweep. Sweep 10-1 was performed with a relatively low inlet steam flow rate, corresponding to the low inlet dewpoint value of 48.5°C and relatively low nitrogen and hydrogen flow rates. This sweep has a relatively high slope on i - V coordinates, indicating a relatively high ASR. This sweep also clearly shows the effects of steam starvation; the slope of the i - V curve increases dramatically as the current density is increased. The outlet dewpoint temperature corresponding to the highest current density shown in this figure was only 4°C for this sweep. Sweep 10-2 was performed at an intermediate steam concentration, with an inlet dewpoint temperature of 70°C. This sweep exhibits nearly linear behavior over the range of current densities shown, with a much smaller slope than sweep 10-1. Sweeps 10-3 and 10-4 are nearly linear at low current densities, then slightly concave-down at higher current densities. Sweep 10-5 has a shallower slope than the others, consistent with the higher operating temperature of 830°C. Sweep 25-1 was performed in a stepwise fashion, rather than as a continuous sweep. This was done in order to ensure sufficient time for the internal stack temperatures to achieve steady-state values at each operating voltage. Note that the slope of this sweep is small, indicating low ASR ($\sim 1.5 \Omega \cdot \text{cm}^2$). This sweep was performed at the beginning of a 1000-hour long-duration 25-cell stack test. Sweep 25-2 was acquired at the end of the long-duration test. The stack operating temperature was increased from 800°C to 830°C part way through the test. Note that the slope of sweep 25-2 is higher than that of sweep 25-1, despite the higher temperature, due to performance degradation over 1000 hours of operation.

The issue of long-term performance degradation is critical if the potential of large-scale hydrogen production based on HTE is ever to be realized. Performance degradation is also an important issue for solid-oxide fuel cells (SOFCs) and addressing this issue has been a major focus of both the US DOE SECA program [21] and the European Real-SOFC program [22]. Significant progress has been made in identifying and mitigating degradation mechanisms in SOFCs. But the electrolysis mode of operation presents some unique possible degradation mechanisms that have received much less attention.

Observations of long-term performance degradation of solid-oxide electrolysis cells have been documented at INL. It should be noted that the INL cells and stacks utilize scandia-stabilized zirconia (ScSZ) electrolyte-supported cells which do not necessarily represent the state-of-the-art in cell design. Furthermore, the scandia dopant level in these cells was only about 6 mol%, which is not high enough to be considered fully stabilized. In addition, ScSZ with dopant levels less than 10% have been shown to exhibit an aging effect with annealing at 1000°C [23].

Long-term degradation in button cell tests can only be due to degradation of the electrodes, the electrolyte, or electrode-electrolyte delamination. There are no effects associated with corrosion, contact resistance, flow fields, or interconnects, since these components are not present. Results of one long-term button-cell test are presented in Fig. 10. This figure shows the area-specific resistance (ASR) of a button cell similar to the one in Fig. 5 plotted as a function of time over the duration of an 1100-hour test. The ASR increases relatively rapidly at the start of the test from an initial value of $\sim 0.6 \Omega \cdot \text{cm}^2$ to a value of $0.9 \Omega \cdot \text{cm}^2$ over about 40 hours. Between 100 hours and 1100 hours, the ASR increases from $0.98 \Omega \cdot \text{cm}^2$ to $1.33 \Omega \cdot \text{cm}^2$. If the initial 100 hours is considered to be a cell conditioning period, the degradation rate over the following 1000 hours is about 35%. This is obviously an unacceptable rate of degradation. As a

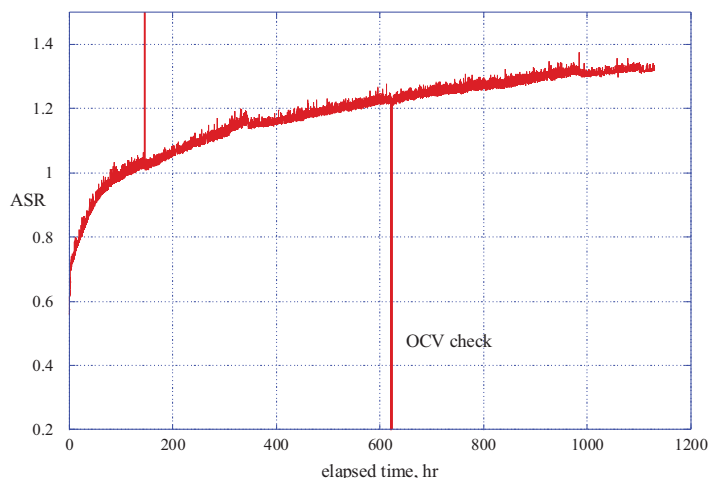


Figure 10. Area-specific resistance of a button cell as a function of time for 1100-hour test.

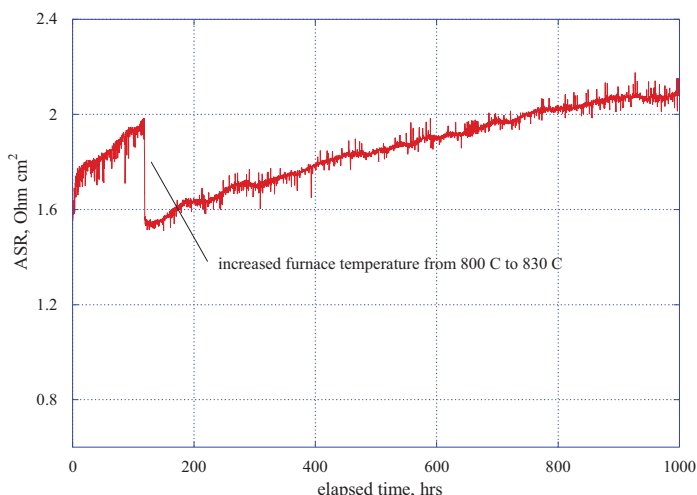


Figure 11. Area-specific resistance of a 25-cell stack as a function of time for a 1000-hour test.

comparison, the Phase-III SECA target degradation rate is 0.1%/1000hr. Several companies are currently coming very close to meeting that target in the SOFC mode of operation.

Performance degradation results with an SOEC stack tested at INL were also presented in reference [5]. Results of a 1000-hour test performed with a 25-cell stack are presented in Fig. 11. This figure provides a plot of the stack area-specific resistance as a function of time for the 1000 hours. The furnace temperature was increased from 800 to 830°C an elapsed time of 118 hours, resulting in a sudden drop in ASR.

The increase in ASR with time represents degradation in stack performance. The degradation rate decreases with time and is relatively low for the last 200 hours of the test. However, from the 118-hour mark to the end of the test, the ASR increased more than 40% over approximately 900 hours. Reduction of this performance degradation is an objective of ongoing research.

One of the objectives of the INL HTE program is technology scale-up and demonstration. To this end, the INL has developed a 15 kW HTE test facility, termed the Integrated Laboratory Scale (ILS) HTE test facility. Details of the design and initial operation of this facility are documented in references [24-26]. A condensed description of the facility will be provided here.

The ILS includes three electrolysis modules, each consisting of four stacks of 60 cells, yielding 240 cells per module and 720 cells total. The cells are similar to those discussed earlier. Each electrolysis module utilizes an independent support system supplying electrical power for electrolysis, a feedstock gas mixture of hydrogen and steam (and sometimes nitrogen), a sweep gas, and appropriate exhaust handling. Each module includes a controlled inlet flow of deionized water, a steam generator, a controlled inlet flow of hydrogen, a superheater, inlet and outlet dewpoint measurement stations, a condenser for residual steam, and a hydrogen vent. All three modules were located within a single hot zone. Heat recuperation and hydrogen product recycle was also incorporated into the facility. A labeled photograph of the ILS is provided in Fig. 12. Each numbered component

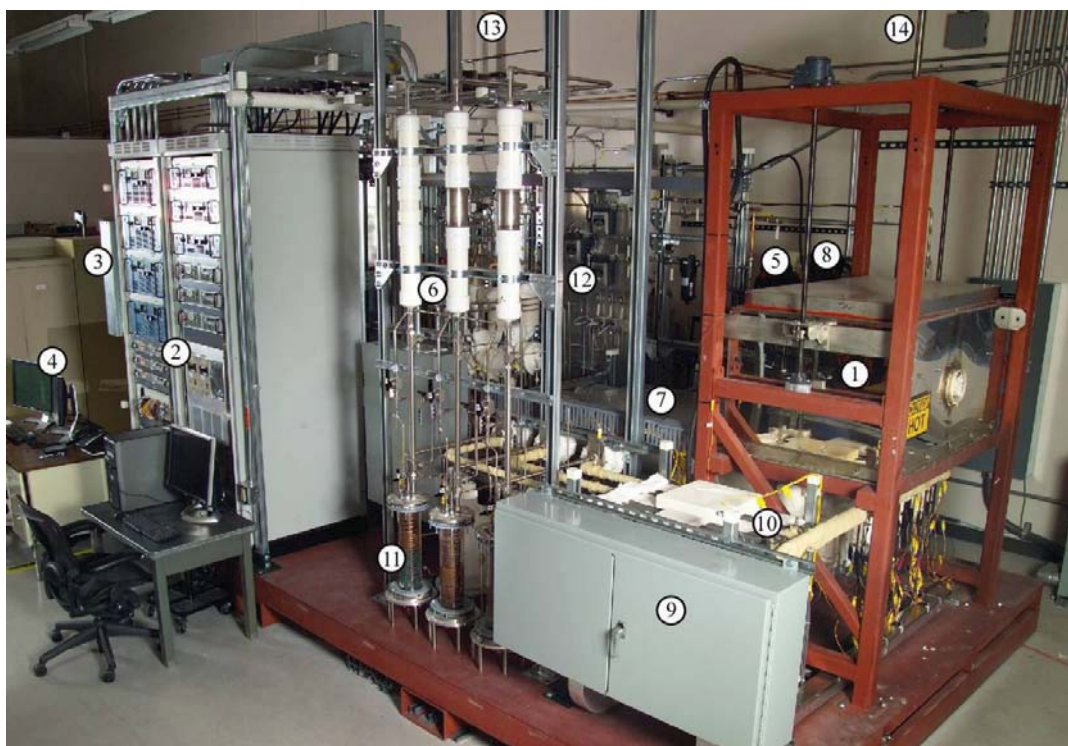


Figure 12. Right side view of INL ILS facility, with major components labeled.

Table 1. Identifiers for Fig. 11.

ID	Component
1	Hot zone enclosure lid
2	Power supply and instrument racks
3	Electrical distribution cabinet
4	Data acquisition and control monitors
5	Deionized water system
6	Steam generator
7	Steam and H ₂ superheaters
8	Air compressor
9	Patch panel
10	Product finned cooler
11	Steam condenser
12	Mass flow controllers
13	H ₂ vent
14	Air and O ₂ vent

is identified in Table 1.

An exploded view of one of the ILS module assemblies including the recuperative heat exchanger, base manifold unit, and four-stack electrolysis unit is presented in Fig. 13. For each four-stack electrolysis module, there were two heat exchangers and one base manifold unit. Each base manifold unit has nine flow tubes entering or exiting at its top and only four flow tubes entering or exiting at the bottom of the unit and at the bottom of the heat exchangers, thereby reducing the number of tube penetrations passing through the hot zone base

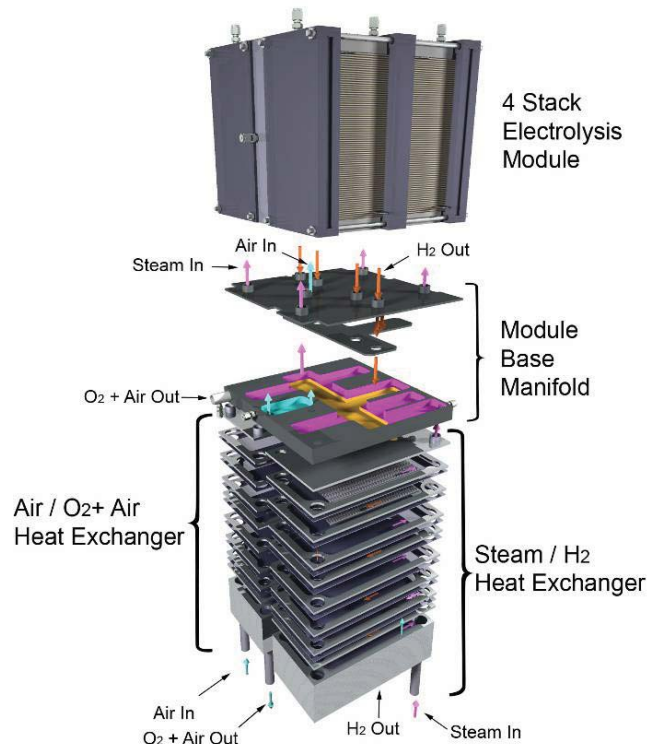


Figure 13. Exploded view of heat exchanger, base manifold unit, and four-stack electrolysis unit.

plate from nine to just four. This feature also reduces the thermal load on the hot zone base plate. An internally manifolded plate-fin design concept was selected for this heat recuperator application. This design provides excellent configuration flexibility in terms of selecting the number of flow elements per pass and the total number of passes in order to satisfy the heat transfer and pressure drop requirements. Theoretical counterflow heat exchanger performance can be approached with this design. This design can also accommodate multiple fluids in a single unit. More details of the design of the recuperative heat exchangers are provided in reference [27].

Fig. 14 shows a rendering of the three ILS electrolysis modules with their base manifolds and heat exchangers beneath. This illustration also shows the instrumentation wires for intermediate voltage and temperature readings. Each module is instrumented with twelve 1/16" sheathed thermocouples for monitoring gas temperatures in the electrolysis module manifolds and in the base manifold. These thermocouples are attached to the manifolds using compression fittings. There are also twelve miniature 0.020" diameter inconel-sheathed type-K thermocouples per module that are used for monitoring internal stack temperatures. Access to the internal region of the stacks is provided via the air outlet face. The internal thermocouples are inserted into the small exit air flow channels. Similarly, seven intermediate voltage tap wires per module are inserted into the air flow channels of the four stacks.

Two compression bars are shown across the top of each module in Fig. 14. These bars are used to maintain compression on all of the stacks during operation in order to minimize electrical contact resistance between the cells, flow fields, and interconnects. The bars are held in compression via spring-loaded tie-downs located outside of the hot zone under the base plate.

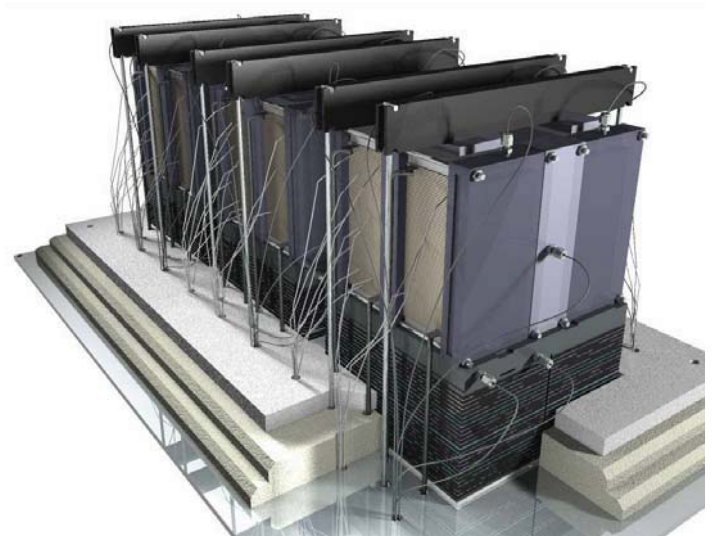


Figure 14. Installation of electrolysis modules, base manifolds and paired heat exchangers.

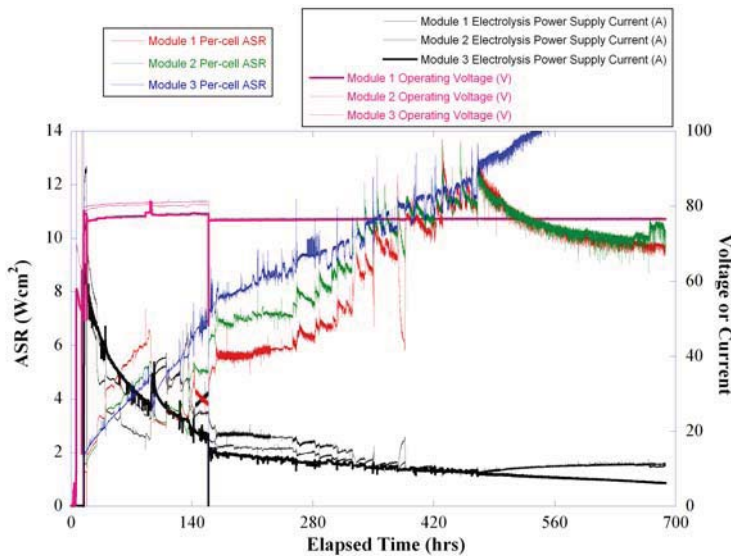


Figure 15. Time history of ILS module ASR values, voltages, and current over 700 hours of operation.

Note that the heat exchangers are partially imbedded in the insulation thickness. The top portion of each heat exchanger is exposed to the hot zone radiant environment, which helps to insure that the inlet gas streams achieve the desired electrolyzer operating temperature prior to entering the stacks. The temperature at the bottom of each heat exchanger will be close to the inlet stream temperature, minimizing the thermal load on the hot zone base plate in the vicinity of the tubing penetrations.

Performance degradation with the ILS system is documented in Fig. 15. Over a period of 700 hours of test time, module-average ASR values increased by about a factor of 5, from an initial value near $1.5 \text{ Ohm}\cdot\text{cm}^2$. Some of the

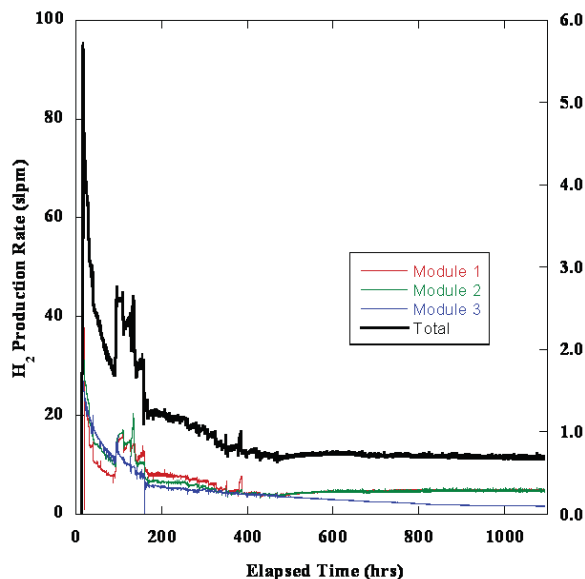


Figure 16. ILS hydrogen production rate time history.

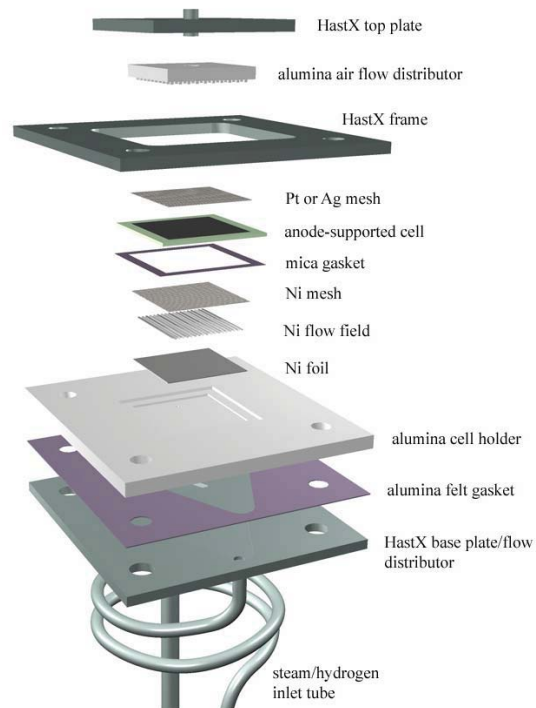


Figure 17. Exploded view of single cell fixture.

observed degradation was related to balance-of-plant issues. For example, prior to about 480 hours of operation, unanticipated condensation occurred in the hydrogen recycle system which led to erratic control of the hydrogen recycle flow rate due to the intermittent presence of liquid water in the mass flow controllers. This problem led to time periods during which there may have been no hydrogen flow to the ILS stacks, leading to accelerated performance degradation associated with oxidation of the nickel cermet electrodes.

Despite the problems with the ILS, we were able to demonstrate large-scale hydrogen production. A plot of the time history of ILS hydrogen production is given in Fig. 16. Peak electrolysis power consumption and hydrogen production rate were 18 kW and $5.7 \text{ Nm}^3/\text{hr}$, respectively, achieved at about 17 hours of elapsed test time.

Single Cell Tests – Anode-Supported Cells

INL is currently in the process of testing several state-of-the-art single $5 \text{ cm} \times 5 \text{ cm}$ anode-supported cells in the electrolysis mode. A new test apparatus has been developed for this purpose. Referring to the exploded view given in Fig. 17, the steam hydrogen mixture enters through the inlet hole in the bottom of the HastX base plate. It then flows through a diverging flow channel milled into the HastX base plate and passes through a slot in the bottom of the alumina cell holder. The steam/hydrogen then flows under the cell through a corrugated/perforated nickel flow field. A nickel foil underneath the flow field will serve as a current collector. A power lead and voltage tap double-ended wire will be spot

welded to the nickel foil and will be situated in one of the grooves of the flow field. These wires will be fed out through holes in the bottom of the alumina cell holder. There will also be a nickel mesh (not shown) in direct contact with the anode above the flow field. A nickel paste will be used to enhance electrical contact between the cell and the nickel mesh, flow field, and foil. The steam-hydrogen flow exits through a slot in the cell holder and then through a converging flow channel

cut into the base plate and out through the steam/H₂ outlet hole in the base plate.

Air is introduced to the cathode side of the cell through holes in the HastX top plate and the alumina air flow distributor. The air flow inlet tube will be welded to the HastX top plate and will protrude into the hole in the alumina air flow distributor. A seal will be formed between the HastX top plate and the alumina air flow distributor by means of a mica gasket or ceramic paste. After exiting the air flow distributor, the air will impinge on the air side of the cell and flow radially outward through an array of protuberances milled into the bottom side of the alumina air flow distributor plate. The air then exits into the furnace volume. A platinum or silver mesh is situated between the air flow distributor and the cathode. A platinum or silver ink will be used to enhance electrical contact between the air electrode and the mesh. A power lead/voltage tap double-ended wire will be spot-welded to the current collector mesh and will be situated in one of the grooves formed by the array of protuberances. It can then be fed out of the fixture from the side.

A fixed compressive load is applied to the entire cell stackup between the alumina cell holder and the HastX top plate by means of weights, as shown in the test stand overview, Fig. 18. This load must simultaneously compress the cell against the mesh, flow field and foil on the steam/hydrogen side and against the seal around the outer edge of the cell. The outer edge of the cell rests on a window frame shelf milled into the alumina cell holder. The seal will be accomplished using a high-temperature SOFC sealing paste. The weight plates are held in alignment by the upper portion of the threaded rods which extend upward for this purpose. There are eight weight plates, each 1.2 lbs, for a total of 9.6 lbs, which yields a compressive pressure of about 20,000 Pa on the cell active area.

A fixed compressive load is independently applied between the HastX frame, the alumina cell holder, and the HastX base plate. This load is generated by the compression of four springs located under the test stand base support outside of the furnace. The springs will be compressed a fixed amount that is determined by the height of the spool pieces. This load is intended to compress the seal between the cell holder and the base plate. This seal will be formed by either a mica gasket or a ceramic sealing paste. A nut is visible on the threaded rod in Fig. 18 just above the HastX frame and below the weight plates. This nut represents the upper stop for this compressive load. The extension of the threaded rods above the nuts is for the purpose of aligning the weight plates. Note that the weight plates are floating above these nuts since they are resting on the HastX top plate.

The air and steam/hydrogen flow tubes will be fabricated from inconel. HastX was specified for the base plate, the frame, and the weight plates. The spacer rods are specified as alumina in order to minimize heat conduction out of the bottom of the furnace.

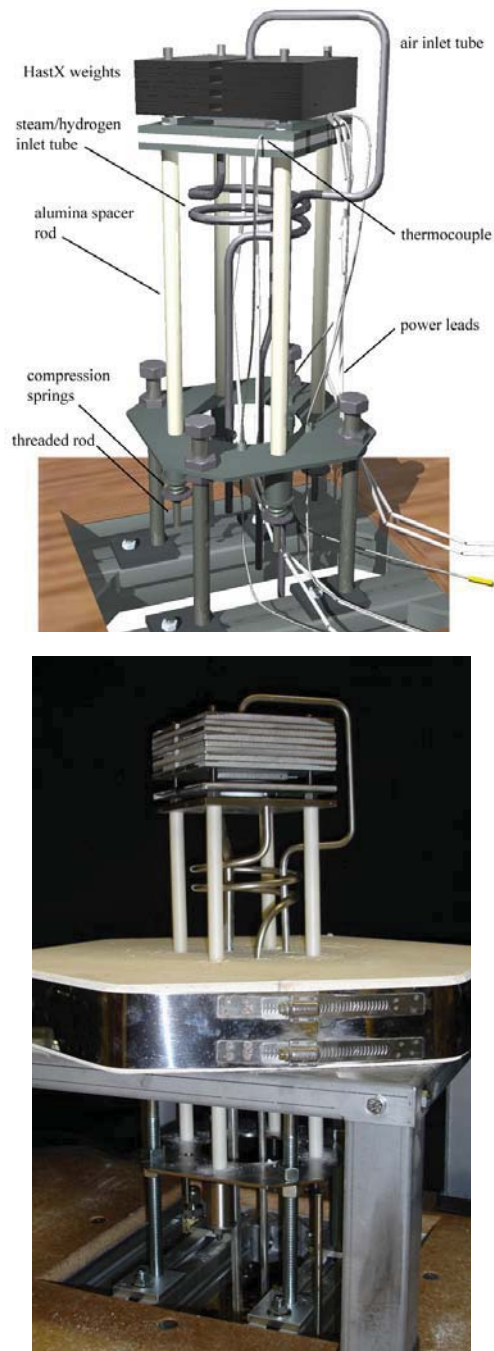


Figure 18. Single-cell test stand for anode-supported cells.

Conclusions

An overview of the high-temperature electrolysis research and development program at the Idaho National Laboratory has been presented, with selected observations of electrolysis cell degradation at the single-cell, small stack and large (15 kW) facility scales. The INL HTE program has successfully demonstrated the potential for high-temperature electrolysis as a large-scale hydrogen production technology. Successful operation of the 15 kW integrated laboratory scale facility for over 1000 hours was completed in the fall of 2008. However, several issues require further research, including cell and stack long-term performance degradation. Degradation has been identified as a major issue that must be solved for high-temperature electrolysis to ultimately achieve any significant level of deployment.

Acknowledgements

This work was supported by the U.S. Department of Energy, Office of Nuclear Energy, Nuclear Hydrogen Initiative and Next Generation Nuclear Plant Programs under DOE Operations Office Contract DE-AC07-05ID14517.

References

1. Forsberg, C. W., "The Hydrogen Economy is Coming. The Question is Where?" *Chemical Eng. Progress*, Dec. 2005, pp. 20-22.
2. Granovskii, M., Dincer, I., and Rosen, M. A., "Greenhouse gas emissions reduction by use of wind and solar energies for hydrogen and electricity production: economic factors," *Int. J. Hydrogen Energy*, Vol. 32, 2007, pp. 927-931.
3. Floch, P-H., Gabriel, S., Mansilla, C., and Werkoff, F., "On the production of hydrogen via alkaline electrolysis during off-peak periods," *Int. J. Hydrogen Energy*, Vol. 32, 2007, pp. 4641-4647.
4. Schultz, K. R., Brown, L. C., Besenbruch, G. E. and Hamilton, C. J., "Large-Scale Production of Hydrogen by Nuclear Energy for the Hydrogen Economy," Report GA-A24265, Feb. 2003, 22p.
5. O'Brien, J. E., Stoots, C. M., Herring, J. S., and Hartvigsen, J. J., "Performance of Planar High-Temperature Electrolysis Stacks for Hydrogen Production from Nuclear Energy," *Nuclear Technology*, Vol. 158, pp. 118 - 131, May, 2007.
6. Steinfeld, A. "Solar thermochemical production of hydrogen," *Solar Energy*, V 78, No 5, pp. 603-615, May 2005.
7. Southworth, F., Macdonald, P. E., Harrell, D. J., Park, C. V., Shaber, E. L., Holbrook, M. R., and Petti, D. A., "The Next Generation Nuclear Plant (NGNP) Project," Proceedings, Global 2003, pp. 276-287, 2003.
8. Schultz, K., Sink, Pickard, P., Herring, J. S., O'Brien, J. E., Buckingham, R., Summers, W., and Michele Lewis, M., "Status of the US Nuclear Hydrogen Initiative," Proceedings of ICAPP 2007, Paper 7530, Nice, France, May 13-18, 2007; *The Nuclear Renaissance at Work*, V. 5, Societe Francaise d'Energie Nucleaire – ICAPP 2007, pp. 2932-2940.
9. Yildiz, B., and Kazimi, M. S., "Efficiency of Hydrogen Production Systems Using Alternative Nuclear Energy Technologies," *Int. J. of Hydrogen Energy*, Vol. 31, pp. 77-92, 2006.
10. O'Brien, J. E., McKellar, M. G., and Herring, J. S., "Performance Predictions for Commercial-Scale High-Temperature Electrolysis Plants Coupled to Three Advanced Reactor Types," 2008 International Congress on Advances in Nuclear Power Plants, June 8-12, 2008, Anaheim, CA.
11. O'Brien, J. E., McKellar, M. G., Stoots, C. M., Herring, J. S., and Hawkes, G. L., "Parametric Study of Large-Scale Production of Syngas via High Temperature Electrolysis," in press, *International Journal of Hydrogen Energy*, 2009.
12. Stoots, C. M., O'Brien, J. E., "Results of Recent High-Temperature Co-electrolysis Studies at the Idaho National Laboratory," in press, *International Journal of Hydrogen Energy*, 2009.
13. Jensen, S. H., Larsen, P. H., Mogensen, M., "Hydrogen and synthetic fuel production from renewable energy sources," *Int. J. Hydrogen Energy*, Vol. 32, pp. 3253-3257, 2007
14. Mogensen, M., Jensen, S. H., Hauch, A., Chorkendorff, Ib., and Jacobsen, T., "Reversible Solid Oxide Cells," *Ceramic Engineering and Science Proceedings*, V 28, n 4, Advances in Solid Oxide Fuel Cells III - A Collection of Papers Presented at the 31st International Conference on Advanced Ceramics and Composites, 2008, p 91-101.
15. O'Brien, J. E., "Thermodynamic Considerations for Thermal Water Splitting Processes and High-Temperature Electrolysis," 2008 ASME International Congress and Exposition, paper# IMECE2008-68880, Boston, Nov., 2008.
16. UniSim Design, R360 Build 12073, Copyright ©2005-2006 Honeywell International Inc.
17. Yildiz, B., and Kazimi, M. S., "Efficiency of hydrogen production systems using alternative nuclear energy technologies," *Int. J. Hydrogen Energy*, Vol. 31, pp. 77-92, 2006.
18. Brown, L. C., Lentsch, R. D., Besenbruch, G. E., Schultz, K. R., "Alternative Flowsheets for the Sulfur-Iodine Thermochemical Hydrogen Cycle," *AIChE Journal*, April 2003.
19. O'Brien, J. E., Stoots, C. M., Herring, J. S., Lessing, P. A., Hartvigsen, J. J., and Elangovan, S., "Performance Measurements of Solid-Oxide Electrolysis Cells for Hydrogen Production," *Journal of Fuel Cell Science and Technology*, Vol. 2, pp. 156-163, August 2005.
20. O'Brien, J. E., Stoots, C. M., Herring, J. S., and Hartvigsen, J. J., "Hydrogen Production Performance of a 10-Cell Planar Solid-Oxide Electrolysis Stack," *Journal*

- of *Fuel Cell Science and Technology*, Vol. 3, pp. 213-219, May, 2006.
21. Williams, M. C., Strakey, J. P., Surdoval, W. A., Wilson, L. C., "Solid oxide fuel cell technology development in the US," *Solid State Ionics*, V. 177, No. 19-25, pp. 2039-2044, Oct. 2006.
 22. Steinberger-Wilkens, R. Tietz, F., Smith, M. J., Mougins, J., Rietveld, B., Bucheli, O., Van Herle, J., Mohsine, Z., and Holtappels, P., "Real-SOFC – A Joint European Effort in Understanding SOFC Degradation," *ECS Transactions*, v 7, n 1 PART 1, *ECS Transactions - 10th International Symposium on Solid Oxide Fuel Cells, SOFC-X*, 2007, pp. 67-76.
 23. Haering, C., Roosen, A., Schichl, H., and Schnoller, M., "Degradation of the electrical conductivity in stabilized zirconia system Part II: Scandia-stabilised zirconia," *Solid State Ionics*, Vol. 176, No 3-4, pp. 261-268, Jan., 2005.
 24. Housley, G., Condie, K., O'Brien, J.E., Stoots, C.M., "Design of an Integrated Laboratory Scale Experiment for Hydrogen Production via High Temperature Electrolysis," paper no. 172431, ANS Embedded Topical: International Topical Meeting on the Safety and Technology of Nuclear Hydrogen Production, Control, and Management, June 24 - 28, 2007, Boston, Massachusetts, USA.
 25. Stoots, C. M., O'Brien, J. E., "Initial Operation of the High-Temperature Electrolysis Integrated Laboratory Scale Experiment at INL," 2008 International Congress on Advances in Nuclear Power Plants, June 8-12, 2008, Anaheim, CA.
 26. Stoots, C. M., O'Brien, J. E., Condie, K., Moore-McAteer, L., Housley, G. K., Hartvigsen, J. J., and Herring, J. S., "The High-Temperature Electrolysis Integrated Laboratory Experiment," *Nuclear Technology*, April, 2009.
 27. Housley, G. K., O'Brien, J. E., and Hawkes, G. L., "Design of a Compact Heat Exchanger for Heat Recuperation from a High Temperature Electrolysis System," 2008 ASME International Congress and Exposition, paper# IMECE2008-68917, Boston, Nov., 2008.